Multivariate Parameter Evaluation of Pharmaceutically Important Cellulose Ethers

BENGT PERSSON, HANS EVERTSSON,* ROLF BERGMAN,† AND LARS-OLOF SUNDELÖF

Contribution from *Physical Pharmaceutical Chemistry, Uppsala University, Uppsala Biomedical Centre, Box 574, 751 23 Uppsala, Sweden, and SPOC, UF3A1, Pharmacia & Upjohn, 751 82 Uppsala.*

Received February 24, 1998. Accepted for publication April 22, 1999.

Abstract □ A set of nonionic cellulose ethers with varying hydrophobicity and molecular weight has been investigated by principal component analysis (PCA). Several experimental variables such as dynamic surface tension, diffusion coefficient, microviscosity as monitored by a fluorescence probe technique, and intrinsic viscosity are included in the analysis. The experimental variables and observations (polymer fractions) are analyzed in models with good predictive capacities. The apparent equilibrium surface tension correlates to the cloud point and to the critical aggregation concentration in the presence of surfactant. The microviscosity is shown to be a predictive parameter for the degree of hydrophobic substitution. The irreversible process of dynamic surface tension is dependent on the diffusion coefficient but to an even larger degree on the polymer concentration, which is well illustrated by the PCA models.

Introduction

Cellulose ethers of amphiphilic nature such as hydroxypropyl(methyl)cellulose (HPMC) and ethyl(hydroxyethyl)-cellulose (EHEC) are widely used in various pharmaceutical dosage forms. These polymers are used as swelling agents, binders, emulsifiers, rheological stabilizers, and for film coating, etc.[1] Cellulose ethers can be obtained in a variety of fractions (samples) with different physicochemical properties, since the molecular weight and degree of substitution can vary considerably. Furthermore, large batch to batch variations are common which may alter the final pharmaceutical product in which they occur. Interaction between these high molecular weight amphiphiles and low molecular weight active substances, which often are hydrophobic or even amphiphilic in nature,[2] will affect, for example, the release rate of drug from pharmaceutical formulations based on cellulose ethers. The strength of such associative polymer−drug interaction is in turn dependent on the physicochemical properties of the cellulose ether used. Thus, it is of importance to map the influence of the chemical structure of the polymer on its physicochemical properties in aqueous solution.

A set of cellulose ethers differing in hydrophobicity has previously been thoroughly examined in this laboratory by time dependent surface tension determination, viscosity measurements, fluorescence probe techniques, solubilization measurements, light scattering techniques, and size exclusion chromatography. Most of these experimental results have been published elsewhere.[3−5] Some qualitative relationships between the observed variables were seen. However, the interplay between a large number of variables is difficult, if at all possible, to reveal without the aid of mathematical tools capable of handling many, even correlated, variables simultaneously.

Multivariate analysis[6] (MVA) has, over the last couple of decades, become more and more important as the amount of data available on chemical systems increases steadily. This branch of science, today named chemometrics when applied on chemistry, involves a number of multivariate methods[6] and is used in various branches of chemistry and chemical processing[7,8] to find optimum conditions. The present polymer systems have been investigated by principal component analysis[6] (PCA), a method based on linear algebra involving a matrix decomposition. Special emphasis has been put on finding models as simple as possible with which to describe the systems, to find predictive parameters for the physicochemical properties of the polymer fractions (samples). Since the experimental data available on these polymer fractions are quite extensive, the paper also presents a validation of the usefulness of principal component analysis on complex aqueous polymer systems.

Experimental Section

Most of the data used in the analysis are published elsewhere.[3−5] The different polymer samples (observations) are six different ethyl(hydroxyethyl)cellulose (EHEC) fractions, CST-103, DVT-87014, E230G, E411G, PR, OS, varying in molecular weight and degree of substitution, and one fraction each of hydroxypropyl-(methyl)cellulose (HPMC), hydroxypropylcellulose (HPC), hydroxyethylcellulose (HEC), and methylcellulose (MC). All EHEC fractions were obtained from Akzo Nobel AB, Stenungssund, Sweden. HEC and MC were obtained from Aldrich Chemie, Steinham, Germany, HPMC from Colorcon., West Point, PA, and HPC from Hercules Inc., Wilmington, DE. The abbreviations of the variables studied are explained in the Glossary.

The determinations of molecular weight, diffusion coefficient, microviscosity, and the rest of the parameters are presented elsewhere.[3−5] The microviscosity of the mixed sodium dodecyl sulfate−polymer micelles was determined with the fluorescent probe 1,3-di(1-pyrenyl)propane, P3P. The intramolecular excimer formation of P3P is dependent on the local microfluidity around the probe, and the monomer to excimer intensity ratio, I_M/I_E, is a qualitative measure of the microviscosity.[9]

Method

Principal component analysis (PCA) was performed using the SIMCA software package.[10] The data matrix was normalized and centered by an autoscaling procedure, before the principal components (PC:s) were calculated. This is a least-squares method producing principal components which are orthogonal to each other. The first principal component represents the largest variation in the data, and the second component describes the second largest variation orthogonal to the first and so forth. The observations (polymer fractions) are in some sense sum-

* Corresponding author. E-mail: hans.evertsson@farmkemi.uu.se.
† Pharmacia & Upjohn.

10.1021/js9804922 CCC: $18.00
Published on Web 06/05/1999

Table 1—Summary of Some of the Experimental Data Used in the Principal Component Analysis. The Variables Are Explained in the Experimental Section

Polymer	M_w (×10^5 g/mol)	MS_{ao}	DS_{alkyl}	CP (°C)	C1 (mM SDS)	IM/IE-max	[η] (mL/g)	D (×10^{-12} m^2/s)	γ (mN/m)
EHEC Fractions									
CST-103	1.89	0.7	1.5	28	1.5	13.2	455	6.59	37
DVT-87014	1.33	0.9	1.4	28	1.5	8.1	290	7.55	40
E230 G	5.35	0.9	0.9	65	3.9	3.2	410	7.65	48
E411 G	7.85	1.7	1.2	58	3.7	3.2	1000	6.3	52
OS	13.2	1.5	1.6	24	1.5	10.0	1400	–	37
PR	12.4	1.75	1.4	48	2.5	4.0	1500	–	42
Other Cellulose Ethers									
HPMC	3.01	0.4	2	55	3.9	5.2	740	6.48	47
HPC	1.06	0.4	–	42	2.0	6.6	134	12.22	42
MC	1.62	–	2	65	4.1	3.1	400	8.37	47
HEC	1.89	3	–	100	7.0	2.4	237	7.55	63

marized in the score vectors, which are linear combinations of the variables, and the corresponding summary of the variables is named loadings. In other words, the original experimental variables are decomposed into fewer new variables (PC:s) onto which the observations are projected. A multiplication of the score (**T**) and loading (**P′**) matrixes plus a residual (**R**) will regain the original normalized and centered data matrix (**X**) according to

$$\mathbf{X} = \mathbf{T}\cdot\mathbf{P}' + \mathbf{R} \qquad (1)$$

The original, unscaled data matrix is given in Appendix 1. The accuracy of the least squares models is expressed as R^2, the explained variance of the model. R^2 is the comparison between the squared sum of the experimental observations (y_{obsd}) and the squared sum of the values calculated by the model (y_{calcd}) according to

$$R^2 = (\sum y_{obsd}{}^2 - \sum (y_{obsd} - y_{calcd})^2)/\sum y_{obsd}{}^2 \qquad (2)$$

where the sums range from 1 to n observations. R^2 increases with the number of PC:s used in the model since more variation in the experimental data can be explained as the number of "new" variables used increases, and hence the residual decreases. The idea with the PCA, however, is to use as few PC:s as possible in order to get a simpler model. Q^2 describes the relation between the squared sum of observed values and the sum of squares of the values as determined from cross validation (y_{cv}):[8]

$$Q^2 = (\sum y_{obsd}{}^2 - \sum (y_{obsd} - y_{cv})^2)/\sum y_{obsd}{}^2 \qquad (3)$$

Cross validation is a process where the data themselves are used. A few data points are left out at a time of the consecutive model-calculations. Each data point is left out of the calculation once. The closer to 1 that Q^2 is, the better the model. The predictive capacity can never be higher than the explained variance and will reach a maximum when increasing the number of PC:s used. Thus, the optimum model has a high R^2 as well as Q^2 and a small difference between the two. It follows that the model only is valid within the experimental domain. All models presented here contain two principal components. The R^2 value for each component is noted in percent on the axes in the figures. The cumulative R^2 and Q^2 for each model are as follows: Figures 1a and 1b (model 1), 0.882 and 0.536; Figures 2a and 2b (model 2), 0.733 and 0.325; Figures 3a and 3b (model 3), 0.769 and 0.648, respectively. The ellipse in each figure describes the 95% confidence region.[10]

Results and Discussion

The characterization of water soluble polysaccharides is far from trivial, involving a number of physically different methods such as in this case dynamic light scattering, fluorescence probe techniques, and dynamic surface tension. Some, but far from all, qualitative relationships can be deduced just by looking at Table 1 and Appendix 1. Principal component analysis, however, gives a much more objective picture of the complex interplay between the variables. The extensive knowledge of the polymer fractions from this laboratory gives the possibility to construct models containing the appropriate parameters, a critical step in the analysis which is always subjective to some degree. The data set has been divided into two subsets; one containing observations of some of the polymer systems at equilibrium (Figures 1a and 1b (model 1)), and one containing observations describing the irreversible process of dynamic surface tension before equilibrium together with part of the equilibrium responses (Figures 2a and 2b (model 2), Figures 3a and 3b (model 3)). The a-figures give the loading plot (experimental variables in relation to the principal components) of each model, and the b-figures give the score plot (polymer samples in relation to the principal components) of each model.

Equilibrium Parameters—Only the EHEC fractions were chosen for the equilibrium parameter model since complete substituent-information exist for these fractions, and the substituents are of the same types ethyl (hydrophobic) and hydroxyethyl (hydrophilic) groups. This makes the EHEC subgroup straightforward to compare. Figure 1a shows the loadings of the experimental variables for two significant principal components (PC:s, denoted p1 and p2 in the figure) for all EHEC fractions. If a variable is located close to and far along a PC axis, this variable "strongly loads" into that PC. Such an experimental variable then correlates with the new variable, or PC. Original experimental variables lying close to each other correlate in the hyper plane (the two-dimensional window provided by p1 and p2). The model shows four groupings of experimental variables located far along the positive and negative sides on the two principal component axes p1 and p2. The first PC monitors the largest variation in the data. It can be interpreted from the figure that the surface tension γ (measured after 11.7 h on 500 ppm polymer solutions) is strongly correlated to the surfactant concentration corresponding to the onset of polymer–surfactant interaction C1, as well as the cloud point CP, since these variable vectors lie close to and far out on the first principal component axis. Also, these variables are negatively correlated to the microviscosity indices and the surface pressure as these variables are grouped close to and far along the negative side of the first principal component. The negative correlation between the microviscosity and CP/C1/γ is in accord with the earlier reports.[4,5] These correlations can be qualitatively deduced from Table 1. Furthermore, CP, C1, the surface tension, and the micro-

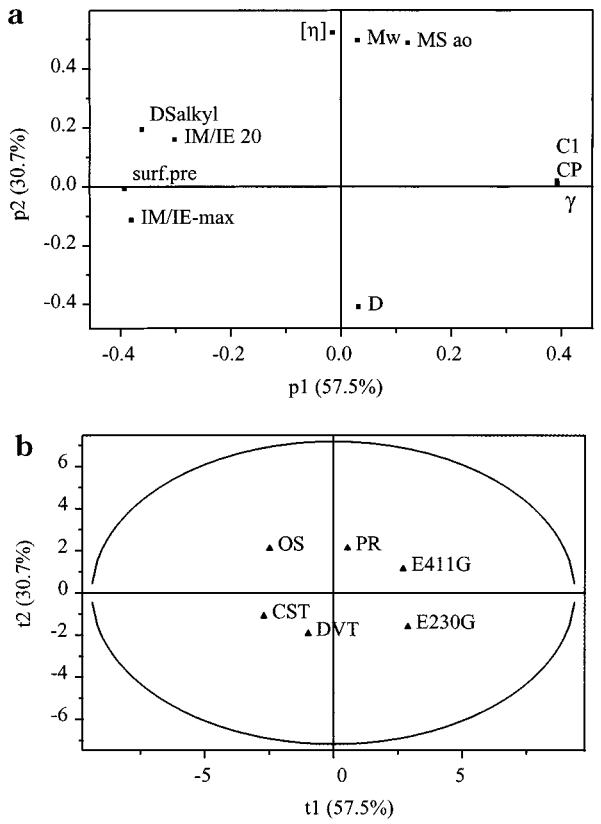

Figure 1—(a) Loading plot of all EHEC fractions of the equilibrium model, showing the first (p1) and second (p2) PC. The cumulative R^2 and Q^2 are 0.882 and 0.536, respectively. (b) The corresponding score plot of all EHEC fractions of the equilibrium model, showing the first (t1) and second (t2) PC.

viscosity are mainly governed by the hydrophobicity of the EHEC fractions, as can be seen by the degree of hydrophobic substitution, DS_{alkyl}, which is located in the group of variables at the negative side of the first principal component axis, and thus correlates with the microviscosity and the surface pressure. A high surface tension, close to that of water, is coupled to a high cloud point as both variables monitor the hydration properties of the polymer. A high surface tension also gives a low surface pressure, or surface activity, since the latter is the difference between the surface tension of water (73 mN/m) and the surface tension of the polymer.

The microviscosity of mixed polymer−surfactant micelles is hence strongly correlated to the hydrophobic substitution of the polymer, as well as the surface activity, which earlier has been discussed[9] in terms of the ability of the polymer to form densely packed mixed polymer−surfactant micelles. This principal component model verifies that the microviscosity of the ternary system EHEC/sodium dodecyl sulfate/water can be used to predict the solubilization properties of the corresponding binary cellulose ether/water system, with the additional information that DS_{alkyl} is the structure-related parameter with the highest influence on the ability to form densely mixed polymer micelles with SDS.

The second PC p2 monitors the second largest variation in data, 30.7%, as compared to the first PC, 57.5%. As expected, the diffusion coefficient D is negatively correlated to the molecular weight and the intrinsic viscosity, which follows directly from the Stokes−Einstein equation $D = kT/(6\pi\eta r)$, where k is the Boltzmann constant, T is the temperature, η is the viscosity of the solvent, and r is the radius of a small hard sphere immersed in the viscous solvent. It should be pointed out that D is obtained by dynamic light scattering, $[\eta]$ from capillary viscometry, and M_w from size exclusion chromatography—that is, from independent methods. The molecular weight correlates as expected with the intrinsic viscosity in accord with the Mark−Houwink equation $[\eta] = KM^a$. These variables, however, do not explain the variation of data along the first PC and hence neither to the surface tension nor to the microviscosity. An interesting feature is that the intrinsic viscosity is correlated to MS_{ao}, the degree of hydrophilic substitution. This is not too surprising since a polymer with a higher hydrophilicity tends to swell in an aqueous solution. MS_{ao} does not occur directly opposite to DS_{alkyl} in the plot. Whereas the degree of hydrophobic substitution has a strong influence on the steady state surface tension and microviscosity, the degree of hydrophilic substitution is important for the intrinsic viscosity. This of course, is not entirely true since DS_{alkyl} and MS_{ao} in combination give the polymer its specific amphiphilic nature. For example, CST-103 is partly self-aggregated in aqueous solution due to the uneven distribution of large hydrophobic substituents,[5,11] a feature originating in the hydrophobic−hydrophilic balance and clearly affecting the hydrodynamics of the polymer. Nonetheless, the degree of hydrophobic substitution DS_{alkyl} seems to affect the microviscosity of polymer/surfactant micelles to a larger extent than the degree of hydrophilic substitution MS_{ao}.

Figure 1b shows the score plot corresponding to the loading plot of Figure 1a. The PC:s are denoted t1 and t2 to signify that the vectors plotted in this space are observables (polymer samples)—not original variables as in the loading plot of Figure 1a, where the PC:s are denoted p1 and p2. The observation vectors in Figure 1b are separated with an even distribution. Such a score plot thus gives a good overview of the observations or polymer samples in relation to the new variables (PC:s), which carry about 88% of the information of the original experimental variables. The two EHEC samples having the highest molecular weight, OS and PR, are located above the others in accord with Figure 1a. The fractions having the higher microviscosities and lower surface tensions, OS and CST-103, are located to the left, also in accord with the loading plot, cf. the original data matrix in Table 1 and Appendix 1. This score plot separates CST from DVT in accord with previous investigations[3−5] even though these two fractions have very similar degree and balance in substitution. The difference is thought to originated in a more separated distribution of substituents and hence longer substituents on the CST fraction, making it effectively more hydrophobic.

The above presented model makes it possible to predict (to 54% using only these six EHEC samples) the solution properties of an unknown EHEC sample by just knowing its DS_{alkyl} and MS_{ao}. If, in addition, some easily measured variable as CP is determined, the other experimental variables can be predicted more precisely and optimum conditions for these determinations might be chosen. Any of the experimental variables along p1 should be useful for the prediction of the strength of amphiphilic polymer−drug interaction, which is important when designing advanced controlled release formulations.

Dynamic Parameters—The irreversible process of surface tension decrease to equilibrium is considered here for all of the cellulose ethers investigated. Figure 2a shows the loadings of the surface tension from time zero to equilibrium at an initial homogeneous polymer concentration of 3 ppm, the lag time, t_{lag}, and the time it takes to reach $(\gamma H_2O - \gamma)/2$, t. t_{lag} is the time from time zero to the point where the surface tension curve shows a negative second derivative. The major variation in data is illustrated along the horizontal first PC axis p1, where the diffusion coefficient is negatively correlated to the surface tension

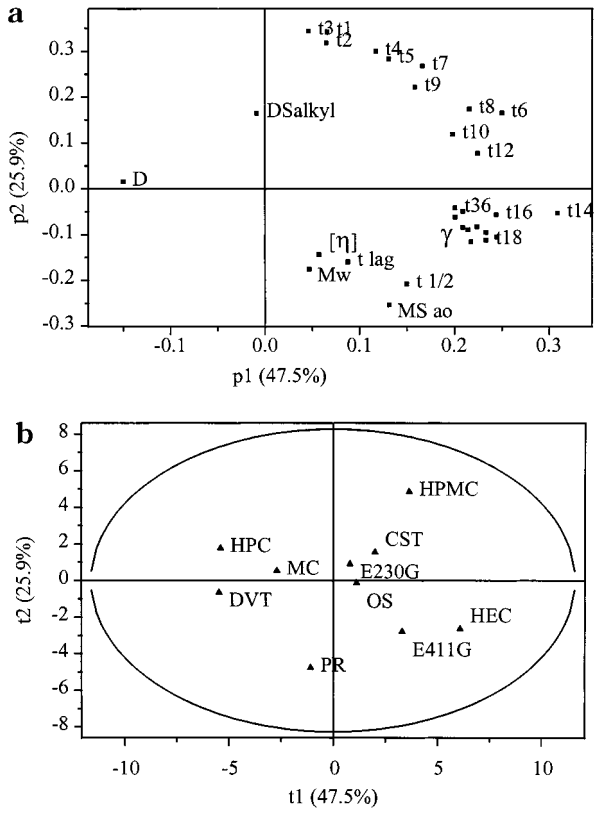

Figure 2—(a) Loading plot of all polymer fractions of the first dynamic model, showing the first (p1) and second (p2) PC. The polymer concentration in the surface tension measurements is 3 ppm. The cumulative R^2 and Q^2 are 0.733 and 0.325, respectively. (b) The corresponding score plot of all polymer fractions of the first dynamic model, showing the first (t1) and second (t2) PC.

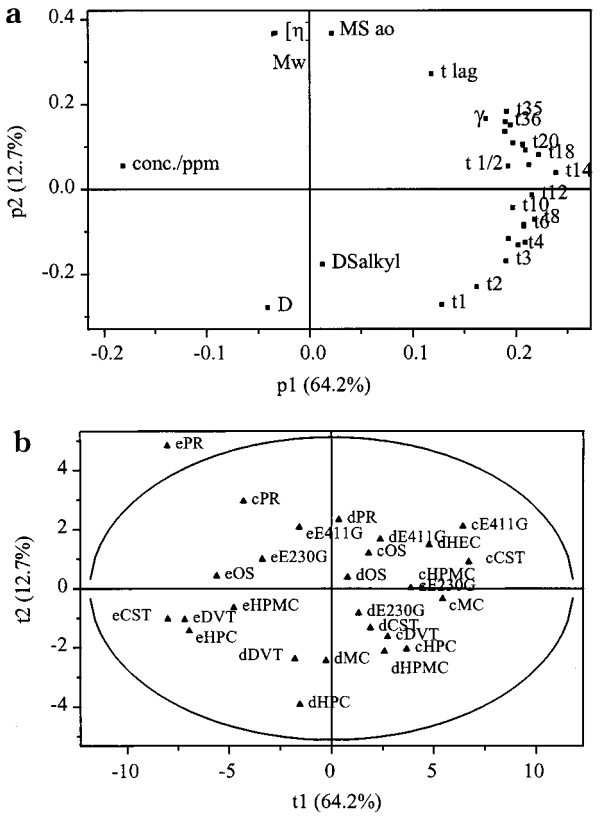

Figure 3—(a) Loading plot of all polymer fractions of the second dynamic model, showing the first (p1) and second (p2) PC. The polymer concentrations in the surface tension measurements are 2, 3, and 10 ppm. The cumulative R^2 and Q^2 are 0.769 and 0.648, respectively. (b) The corresponding score plot of all polymer fractions of the second dynamic model, showing the first (t1) and second (t2) PC. The prefix of each observation corresponds to the polymer concentrations of the surface tension measurements: c = 2 ppm, d = 3 ppm, e = 10 ppm.

at ascending times, meaning that a large diffusion coefficient gives a low surface tension after a certain time. A clear trend within the surface tension variables at ascending times is seen. The early times are located at the top of the plot and a movement downward of the second PC and to the right is seen as the time increases. At very early times the surface tension vectors are totally random due to randomness (a low signal-to-noise ratio) in the measurements, and as time evolves, the discrepancy between the scalars (numerical values) constituting the vectors becomes more stable as the surface tension is lowered by polymer adsorption, which tends to relocate the vectors in the hyper plane (the two-dimensional window provided by p1 and p2). The variable vectors t14 (after about 100 min) to γ (measured at 11.7 h) are located as one cluster indicating they are similar. At these longer times the surface tension has reached the lower plateau of the sigmoidal relationship between the surface tension and time[4] for most of the polymers, and the surface tension does not change very much with time in this time interval. The loading plot thus expresses an excellent overview of the irreversible surface tension build up process.

DS_{alkyl} and MS_{ao} span the second principal component p2 in this model as DS_{alkyl} is located in the upper and MS_{ao} in the lower half of the plot. MS_{ao} is still located quite close to the molecular weight and the intrinsic viscosity in accord with the equilibrium model. The molecular weight and the hydrodynamic volume (proportional to $[\eta]$) are also correlated to the lag time and to some extent to the time it takes to reach $(\gamma H_2O - \gamma)/2$, which seems logical; a long lag time should be coupled to a high molecular weight and to slow diffusion. These times also seem to be dependent on the amount of hydrophilic substitutents in accord with Figure 1a and the discussion above.

The corresponding score plot is given in Figure 2b. The more hydrophilic fractions PR, HEC, and E411 G are located far down in the plot, and the fast-diffusing substances DVT, HPC, and MC to the left, cf., the original data matrix in Appendix 1, and Table 1. The position of each observation in this score plot thus represents a fingerprint of the dynamic behavior of each polymer fraction, since all experimental variables are decomposed into these two principal components t1 and t2.

A conclusion from the dynamic model of Figures 2a and 2b is that the time dependence of the surface tension process is dependent on the molecular weight of the polymer samples to a large extent, which in turn is easily determined from the intrinsic viscosity.

The speed of the irreversible process of dynamic surface tension will, of course, also be dependent on the polymer concentration initially present in the bulk. To determine the effect of the polymer concentration, a second model containing the dynamic parameters is given in Figures 3a and 3b. This model is based on the same data set as above, with time dependent surface tension data at two additional polymer concentrations, 2, 3, and 10 ppm. Hence, the influence of polymer concentration on the irreversible time dependent surface tension process is presented here. In the loading plot of Figure 3a, the main variation in data along the first PC p1 is strongly governed by the polymer concentration. An increase in the polymer concentration results in a decrease in the surface tension after a certain time since the two quantities are negatively correlated. For example: for CST at t2 (100 s after the start of the experiment) the surface tension is 72.55 mN/m at an initial

polymer concentration of 2 ppm, 71.86 mN/m at 3 ppm, and 64.10 mN/m at 10 ppm.

The polymer concentration affects the dynamics to a much larger extent than what the diffusion coefficient does.[12,13] This is logical in the sense that the net mass transport increases to the surface with increasing polymer concentration, assuming a constant diffusion coefficient. According to Fick's first law of diffusion, the mass flux J of a substance per unit area and time is proportional to the diffusion coefficient and to the concentration gradient of the substance, $J = -D\partial c/\partial x$. This implies the amount of the concentration gradient to increase as the polymer concentration increases. It must be remembered though that the process of polymer adsorption to the water/air interface is more complex than free diffusion, involving different states of chemical potential of the polymer in solution compared to the same polymer at the surface, and a negative concentration gradient at longer times.[12,13] The effect however, is a faster lowering of the surface tension if the mass transport to the surface increases.

This second dynamic model of Figures 3a and 3b shows the same general trends concerning the position of the rest of the variable vectors as the dynamic model of Figures 2a and 2b presented above. The second PC p2 in Figure 3a is dominated by the hydrophobicity of the polymer. The apparent equilibrium surface tension γ is located in the upper half of the plot as is the degree of hydrophilic substitution MS_{ao}, in agreement with the discussion above. Furthermore, this model monitors a difference between t and t_{lag}. While the former is governed by the polymer concentration, the latter is more influenced by the hydrophobic balance of the polymer. In the ideal case this is supported by the experimental data, interpreted as follows: An increase in the polymer concentration lowers both the lag time and the time it takes to reach $(\gamma H_2O - \gamma)/2$, but t_{lag} is also in model 3 independently significantly affected by the amphiphilic character of the polymer, with higher lag times for more hydrophilic, slower diffusing polymer fractions. The lag time thus contains valuable structure-information which, in relation to $t_{1/2}$, helps to interpret the hydrodynamics and surface-related thermodynamics of the polymer. The time it takes to lower the surface tension to $t_{1/2}$, on the other hand, is strongly governed by the mass flux J. In conclusion, t_{lag} is more sensitive to the diffusion coefficient which in turn is decided by the hydrodynamic volume, while $t_{1/2}$—governed by the mass flux J—is more sensitive to the polymer concentration.

Turning next to the score plot in Figure 3b, this plot at first looks more "crowded" and complex to deduce. The main variation in data along the first PC t1 due to different polymer concentrations can be seen to be quite structured, however. The prefix of each observation vector corresponds to a certain polymer concentration; c = 2 ppm, d = 3 ppm, and e = 10 ppm. The observations at 10 ppm is located to the left of the figure in accord with the loading plot. CST spans the first PC more than any other polymer fraction, as eCST is located to the far left, and cCST to the far right of the plot. The dynamic surface tension process of CST is in other words more affected by an increase in the polymer concentration than any of the other polymer fractions, e.g., E411 G or DVT. This is most likely due to a more complex adsorption process and reorientation of CST at the surface, which might be attributed to the tendency for self-aggregation.[11] For most of the polymers, the observation with prefix d (= 3 ppm) is located both below the one with prefix c (= 2 ppm) and e (= 10 ppm). This "minimum" in the majority of the observations suggests 3 ppm to be an optimum concentration for the polymer-characterization using dynamic surface tension, since the correlation to the diffusion coefficient and the hydrophobic substitution reaches a maximum—that is, the influence of diffusion on the surface tension process is best described at 3 ppm.

Summary

In summary, the principal component analysis gives an excellent overview of the complex interaction pattern of nonionic cellulose ethers in aqueous solution and verifies the earlier stated qualitative relationships in a more quantitative manner. However, the good models are obtained from the extensive information and knowledge available on these polymer fractions, which enables choice of the appropriate variable settings. The polymer fractions analyzed constitute a heterogeneous group of substances with polydisperse molecular weights ranging from about one hundred thousand to over a million, large differences in the degree of substitution, and documented complex hydrodynamic behavior such as self-aggregation (CST-103[11]) and intermolecular aggregation—formation (E230 G[3]). Despite this and a few missing data, the models obtained have good predictive capacities and manifest the importance of accurate data handling for the characterization of pharmaceutically important polymer fractions. The influence of hydrophobic balance and molecular weight on the experimental variables is clearly illustrated, making the models useful for synthesis of desirable nonionic cellulose ether fractions. For example, the study displays some important differences between the influence of hydrophobic and hydrophilic substitution on the thermo- and hydrodynamics of the polymer samples.

Glossary

DS_{alkyl}	degree of hydrophobic substitution by alkyl groups (the mean number of alkyl groups per anhydroglucose unit of the polymer) as given by the producer. DSalkyl can be 3 at most, as there are three hydroxyl groups on each anhydroglucose unit of cellulose to etherificate
MS_{ao}	degree of hydrophilic substitution (molar substitution) by alkylene oxide groups (the mean number of alkylene oxide groups per anhydroglucose unit of the polymer) as given by the producer. MS_{ao} can theoretically be larger than 3 due to formation of oligo(alkylene oxide) substituents, but is practically only a small number
M_w	molecular weight as determined by size exclusion chromatography with LALLS/RI detection[3]
D	diffusion coefficient as determined from dynamic light scattering[3]
$[\eta]$	intrinsic viscosity as determined from capillary viscometry[3]
γ	apparent equilibrium surface tension as determined by the pendant drop method[4] measured after 11.7 h
surf. press.	the surface tension of water (γH_2O) minus γ
t1—t35	dynamic surface tension before equilibrium at ascending times. The real times in seconds are regained taking (index number × 5)[2], e.g., for t2: $(2 \times 5)2 = 100$ s
t_{lag}	lag time of surface tension, defined as the time it takes to visually detect a negative second derivative of γ

Appendix 1— The Original Data Matrix Used in the Analysis. The Abbreviations of the Experimental Variables and Observations Are Explained in the Experimental Section

batch	concn ppm	CP (°C)	DS_{alkyl}	MS_{ao}	IM/IE -max	IM/IE 20	C1 (mM)	surf. press.	γ (mN/m)	D	$[\eta]$ (mL/g)	t_{lag} (min)	$t_{1/2}$ (min)	mw	t1	t2	t3	t4
cCST	2	28	1.5	0.7	13.2	3.7	1.5	9.1	63.7	6.59	455	60	210	1.89	72.97	72.55	72.95	72.716
cDVT	2	28	1.4	0.9	8.1	1.8	1.5	25.2	47.6	7.55	290	35	249	1.33	73.82		72.44	73.048
cE230G	2	65	0.9	0.9	3.2	2	3.9	7.6	65.2	7.65	410	20	138	5.35	72.36	72.73	71.31	70.95
cE411G	2	58	1.2	1.7	3.2	2.2	3.7	11.9	60.9	6.3	1000	77.5	240	7.85	74.65		72.76	
cOS	2	24	1.6	1.5	10	4	1.5	24.8	48		1400			13.2	72.37	71.69	72.27	70.97
cPR	2	48	1.4	7.75	4	2.2	2.5	17.8	55		1500			12.4	66.9	61.08	58.28	53.52
cHPMC	2	55	2	0.4	5.2	2.2	3.9	18.8	54	6.48	740	84	273.6	3.01	72.05	71.44	71.94	71.878
cHPC	2	42		0.4	6.6	3.9	2	18.5	54.3	12.22	134	40	168	1.06	73.05	72.025	71.97	72.747
cMC	2	65	2		3.1	1.5	4.1	12.8	60	8.37	400	60	234	1.62	73.82	73.483	74.48	72.866
cHEC	2	100		3	2.4	1.5	7			7.55	237			1.89				
dCST	3	28	1.5	0.7	13.2	3.7	1.5	21	51.8	6.59	455	24	63	1.89	72.03	71.86	71.92	70.65
dDVT	3	28	1.4	0.9	8.1	1.8	1.5	30.6	42.2	7.55	290	10	57	1.33	69.81	69.24	69.60	68.10
dE230G	3	65	0.9	0.9	3.2	2	3.9	20.1	52.7	7.65	410	16	89	5.35	72.53		73.33	71.65
dE411G	3	58	1.2	1.7	3.2	2.2	3.7	17.9	54.9	6.3	1000	50	144	7.85	69.31	68.74	68.88	69.21
dOS	3	24	1.6	1.5	10	4	1.5	27.8	45		1400	40	150	13.2	71.698	71.216	71.147	71.913
dPR	3	48	1.4	1.75	4	2.2	2.5	23.8	49		1500	60	180	12.4	67.74	68.07	67.38	67.31
dHPMC	3	55	2	0.4	5.2	2.2	3.9	23	49.8	6.48	740	32	123	3.01	75.39	74.75	75.03	74.324
dHPC	3	42		0.4	6.6	3.9	2	27.3	45.5	12.22	134	7	60	1.06	71.92	71.94	71.68	71.54
dMC	3	65	2		3.1	1.5	4.1	23.8	49	8.37	400	12	56	1.62	71.49	71.745	71.24	70.215
dHEC	3	100		3	2.4	1.5	7	9	63	7.55	237	13		1.89	71.1		70.13	
eCST	10	28	1.5	0.7	13.2	3.7	1.5	37.8	40	6.59	455		30	1.89	69.113	64.104	56.978	52.117
eDVT	10	28	1.4	0.9	8.1	1.8	1.5	30.6	42.2	7.55	290		32	1.33	70.93	66.061	57.94	52.24
eE230G	10	65	0.9	0.9	3.2	2	3.9	22.4	50.4	7.65	410		21	5.35	67.37	63.12	59.65	56.36
eE411G	10	58	1.2	1.7	3.2	2.2	3.7	19	53.8	6.3	1000		24	7.85	71.36	68.043	63.53	57.575
eOS	10	24	1.6	1.5	10	4	1.5	30.3	42.5		1400			13.2	72.54	70.48	66.69	61.52
ePR	10	48	1.4	1.75	4	2.2	2.5	27.8	45		1500			12.4	50.12	48.76	48.74	48.25
eHPMC	10	55	2	0.4	5.2	2.2	3.9	26	46.8	6.48	740		15	3.01	68.98			
eHPC	10	42		0.4	6.6	3.9	2	28.6	44.2	12.22	134		14	1.06	69.01	61.554	52.11	48.358
eMC	10	65	2		3.1	1.5	4.1	21.8	51	8.37	400		35	1.62	71.3		61.59	
eHEC	10	100		3	2.4	1.5	7	9	63	7.55	237		8.4	1.89	70.07		69.22	
gCST	500	28	1.5	0.7	13.2	3.7	1.5	35.8	37	6.59	455			1.89	45.404	45.422	43.663	
gDVT	500	28	1.4	0.9	8.1	1.8	1.5	32.8	40	7.55	290			1.33	43.58		43.01	
gE230G	500	65	0.9	0.9	3.2	2	3.9	24.7	48.1	7.65	410			5.35	52.58	51.552	51.01	50.358
gE411G	500	58	1.2	1.7	3.2	2.2	3.7	21.8	51	6.3	1000			7.85	54.35	53.556	53.59	53.617
gOS	500	24	1.6	1.5	10	4	1.5	35.8	37		1400			13.2	40.76	40.71	40.64	40.25
gPR	500	48	1.4	1.75	4	2.2	2.5	30.8	42		1500			12.4				
gHPMC	500	55	2	0.4	5.2	2.2	3.9	25.4	47.4	6.48	740			3.01	53.9		52.09	
gHPC	500	42		0.4	6.6	3.9	2	31.8	41	12.22	134			1.06	43.43	42.999	42.94	43.13
gMC	500	65	2		3.1	1.5	4.1	27.5	45.3	8.37	400			1.62	55.819	55.164	55.717	
gHEC	500	100		3	2.4	1.5	7	9	63	7.55	237			1.89				

batch	t5	t6	t7	t8	t9	t10	t12	t14	t16	t18	t20	t21	t23	t26	t30	t33	t35	t36
cCST	74.49	72.842	73.18	72.804	73.43	72.911	73.26	71.52	71.52	70.587	70.59	70.341	70.44	67.74	66.37	65.73	65.1	64.45
cDVT	72.13	71.62	71.24	71.324	71.14	71.535	66.84	65.302	64.01	62.405	59.86	58.801	56.6	53.39	50.94		48.83	
cE230G		72.62		72.25	69.8	69.81	68.36	66.58	66.17	66.04	64.17	62.88	60.81	59.55	57.09	57.15	56.89	56.52
cE411G		72.84			72.88		73.97		71.73		69.75		66.8	63.75	62.02	61		60.9
cOS		69.17		69.6		68.33	67.07	64.14	62.97			58.04	54.58	51.61	48.9			
cPR		51.19		50.19		49.022	49.37	48.979	48.69			48.18	47.62	47.54	47.48			
cHPMC	71.537	71.19	71.709	70.491	70.599	70.3	71.342	70.771	68.509	68.241	66.98	67.194	62.96	58.54		54.846	54.301	54.34
cHPC	72.963	71.75	71.593	72.227	70.723	71.47	69.15	68.097		67.121	64.94	63.334	61.42	58.23	56.14	55.372	54.481	54.02

cMC	74.05	72.575	73.23	72.913	72.48	71.481	72.3		70.55	68.383	56.86		64.34	62.28	60.76	60.34	59.3	60.17
cHEC																		
dCST	71.42	71.30	70.78	70.63	70.27		66.95	65.14			60.73		56.64	54.90	52.31	51.56	51.71	51.81
dDVT	68.42	66.10	64.84	64.79	63.44	62.14	59.59			51.53		48.20	46.96	45.04	44.60	44.76	44.14	43.56
dE230G	71.21	71.23	69.16	68.39	66.34	65.18	62.94	60.48	58.92	58.48	56.41	56.69	55.60	53.66	52.52	53.91	52.67	52.67
dE411G		71.00		67.96	68.08		67.23	67.09	63.73	63.57	60.89	59.62	57.91	55.66	55.28	54.28		
dOS		70.516	70.286		69.118		66.275	64.294	62.631	60.496		56.568	53.82	49.137		46.566	46.377	46.189
dPR		66.6		65.32		63.85	62.1	60.67	59.24			54.39	52.2	50.04	49.05			
dHPMC	73.49	74.11	73.705	73.825	72.254	72.21	68.696	65.102	61.725	58.838	56.9	55.045	52.48	51.26	50.38			
dHPC	68.79	67.48	67.33	65.49	63.73	61.77	58.59	53.99	50.81	49.06	47.68	47.25	46.41		45.50	45.57	45.60	45.91
dMC	69.84	67.735	66.66	64.55	63.97	62.259	59.79	57.711	55.57	55.176	53.4	52.752	51.48	50.04	49.21	48.92	48.81	49.05
dHEC	69.32		68.28		65.35		65.05		64.93		65.63		64.29	64.58	64.45	63.07	63.66	62.53
eCST	49.144	47.203	45.089	44.016	43.266	42.451	41.934	41.637	41.314	40.901	40.837	40.591	40.454	40.532	40.059	40.058	39.595	39.983
eDVT	48.76	46.83	45.57	44.55	44	43.694	43.23		42.9	42.895	42.57	42.51	42.23	42.39	42.51	41.843	41.78	41.927
eE230G		54.59	53.41	53.19	52.82		52.51	52.2	51.91	51.95	51.73	51.63	51.34	50.41	50.97	50.03	50.38	50.39
eE411G		57.52	56.641	56.247	55.77		55.45	54.883	54.92	54.637	54.56	53.936	54.73	53.57	53.53	54.258	53.78	53.792
eOS		51.71		46.73		45.22	44.58	44.36	44.16			43.73	43.51	42.96	43.08			
ePR		48.46		47.11		47.42	46.77	46.94	46.76			46.07	45.64	45.81	45.64			
eHPMC	51.03					48.07					47.04		47.51	47.14			46.92	47.2
eHPC	48.91	46.18	46.273		45.36	45.65	45.02			45.15	44.52	44.587	44.68	44.66	44.27	44.16	44.35	44.47
eMC		54.04			50.76		51.13		51.14		50.93		50.87					
eHEC		68.73			67.29		66.07		64.48		66.58		65.36					
gCST	42.618		41.844		41.352		40.878		40.457	40.225	39.668	39.824	39.486	39.346	38./793	38.106	38.289	38.065
gDVT	42.4		42.17		41.82		41.36	41.417	41.37	40.956	40.92	40.662	40.92	40.85	40.07	40.71	40.07	40.29
gE230G	50.51	50.317			50.04		49.68	48.62	48.78	49.523	48.55	48.366	48.58	48.12	58.01	47.98	48.287	48.16
gE411G	53.59		53.25		53.18		52.6	52.311	52.1		52.77	51.826	51.62	52.14	51.9	51.93	51.95	51.7
gOS		40.36		39.96		39.73	39.79	39.83	39.51			39.63	38.96	39.17	38.61			
gPR																		
gHPMC	51.13		50.97		50.22		49.95				49.53		49.05	48.7	48.6	47.75	48.39	48.76
gHPC	42.52	42.203	41.81	41.758	41.67	41.236	41.73		41.37	41.894	41.39	41.762	42.01	41.83	41.34	41.64	41.19	41.84
gMC	55.075		55.042		55.025		55.051	51.075	50.34		47.968	49.494	48.619	47.248	46.557	45.711	45.264	45.42
gHEC																		

$t_{1/2}$	the time it takes to reach ($\gamma H_2O - \gamma$)/2
concn/ppm	the polymer concentration in ppm. Because the low concentrations and measurements carried out at room temperature, 1 ppm = 1×10^{-4} (w/v)%
CP (°C)	the cloud point temperature[3]
C1 (mM)	the surfactant (SDS) concentration at onset of polymer−surfactant interaction[5]
$I_{M/IE-max}$	the maximum monitored value of the microviscosity of polymer−surfactant mixed micelles as monitored by the fluorescent probe P3P[5] in SDS/0.2% polymer/water solutions
$I_{M/IE20}$	an asymptotic value of $I_{M/IE}$ for 20 mM SDS/0.2% polymer/water solutions

References and Notes

1. *Handbook of Pharmaceutical Excipients*; Wade, A., Weller, P. J., Eds.; American Pharmaceutical Association & The Pharmaceutical Press: London, 1994.
2. Attwood, D.; Florence, A. T. *Surfactant Systems*; Chapman & Hall: Bristol, 1983.
3. Nilsson, S.; Sundelöf, L.-O.; Porsch, B. On the Characterization Principles of Some Technically Important Water Soluble Nonionic Cellulose Derivatives. *Carbohydr. Polym.* **1995**, *28*, 265−275.
4. Persson, B.; Nilsson, S.; Sundelöf, L.-O. On the Characterization Principles of Some Technically Important Water Soluble Nonionic Cellulose Derivatives. Part II: Surface Tension and Interaction With a Surfactant. *Carbohydr. Polym.* **1996**, *29*, 119−127.
5. Evertsson, H.; Nilsson, S. Microviscosity in Dilute Aqueous Solutions of SDS and Nonionic Cellulose Derivatives of Different Hydrophobicity: Fluorescence Probe Investigations. *Carbohydr. Polym.* **1998**, *35*, 135−144.
6. Mardia, K. V.; Kent, J. T.; Bibby, J. M. *Multivariate analysis*; Academic Press: Great Yarmouth, 1989.
7. Sjöström, M.; Wold, S.. In *Chemometrics, Theory and Applications;* American Chemical Society Symposium Series 52; Kowalsky, B., Ed.; American Chemical Society: Washington, D.C., 1977.
8. *Anvendelse av kjemometri innen forskning og industri*; Nortvedt, R., Brakstad, F., Kvalheim, O. M., Lundstedt, T., Eds.; Norsk Kjemisk Selskaps & Svenska Kemistsamfundet: Bergen, 1996.
9. Evertsson, H.; Nilsson, S. Microviscosity in Clusters of Ethyl Hydroxyethyl Cellulose and Sodium Dodecyl Sulfate Formed in Dilute Aqueous Solutions As Determined with Fluorescence Probe Techniques. *Macromolecules* **1997**, *30*, 2377−2385.
10. SIMCA, http://www.umetri.se, Umetri, Box 7960, SE 907 19 Umeå, Sweden.
11. Evertsson, H.; Nilsson, S.; Holmberg, C.; Sundelöf, L.-O. Temperature Effects on the Interactions between EHEC and SDS in Dilute Aqueous Solutions. Steady-State Fluorescence Quenching and Equilibrium Dialysis Investigations. *Langmuir* **1996**, *12*, 5781−5789.
12. Ward, A. F. H.; Tordai, L. Time-Dependence of Boundary Tensions of Solutions. *J. Chem. Phys.* **1946**, *14*, 453−461.
13. Chang, S. A.; Gray, D. G. The Surface Tension of Aqueous Hydroxypropyl Cellulose Solutions. *J. Colloid Interface Sci.* **1978**, *67*, 255−265.

Acknowledgments

Dr. Torbjörn Lundstedt is gratefully acknowledged for valuable discussions. This work has been financially supported by the Swedish Natural Science Research Council and the Swedish council for the Engineering Sciences.

JS9804922